Check for updates

Geophysical Research Letters

RESEARCH LETTER
10.1029/2023GL106693

Assessment of the Madden-Julian Oscillation in CMIP6 Models Based on Moisture Mode Theory

Qiao-Jun Lin[1], **Víctor C. Mayta**[1], **and Ángel F. Adames Corraliza**[1]

[1]Department of Atmospheric and Oceanic Sciences, University of Wisconsin, Madison, WI, USA

Key Points:

- Madden-Julian Oscillation (MJO) simulation skill in 25 Coupled Model Intercomparison Project Phase 6 models is assessed using moisture mode theory
- No model can realistically reproduce all the moisture mode properties of the MJO over the Indian Ocean
- Models that best capture the MJO's moisture mode features exhibit more realistic mean states and MJO structure and propagation features

Supporting Information:

Supporting Information may be found in the online version of this article.

Correspondence to:

Q.-J. Lin,
qiaojun.lin@wisc.edu

Citation:

Lin, Q.-J., Mayta, V. C., & Adames Corraliza, Á. F. (2024). Assessment of the Madden-Julian Oscillation in CMIP6 models based on moisture mode theory. *Geophysical Research Letters*, *51*, e2023GL106693. https://doi.org/10.1029/2023GL106693

Received 5 OCT 2023
Accepted 30 MAR 2024

Author Contributions:

Conceptualization: Qiao-Jun Lin, Víctor C. Mayta, Ángel F. Adames Corraliza
Formal analysis: Qiao-Jun Lin, Víctor C. Mayta, Ángel F. Adames Corraliza
Supervision: Qiao-Jun Lin, Víctor C. Mayta, Ángel F. Adames Corraliza
Writing – review & editing: Qiao-Jun Lin, Víctor C. Mayta, Ángel F. Adames Corraliza

© 2024. The Authors.
This is an open access article under the terms of the Creative Commons Attribution License, which permits use, distribution and reproduction in any medium, provided the original work is properly cited.

Abstract The moist processes of the Madden-Julian Oscillation (MJO) in the Coupled Model Intercomparison Project Phase 6 models are assessed using moisture mode theory-based diagnostics over the Indian Ocean (10°S–10°N, 75°E–100°E). Results show that no model can capture all the moisture mode properties relative to the reanalysis. Most models satisfy weak temperature gradient balance but have unrealistically fast MJO propagation and a lower moisture-precipitation correlation. Models that satisfy the most moisture mode criteria reliably simulate a stronger MJO. The background moist static energy (MSE) and low-level zonal winds are more realistic in the models that satisfy the most criteria. The MSE budget associated with the MJO is also well-represented in the good models. Capturing the MJO's moisture mode properties over the Indian Ocean is associated with a more realistic representation of the MJO and thus can be employed to diagnose MJO performance.

Plain Language Summary The Madden-Julian Oscillation (MJO) is arguably the most important tropical phenomenon that drives weather at the intraseasonal time scale. Although the MJO has been analyzed for the past decades, its simulation in climate models can still be improved. Previous studies have emphasized that the MJO evolution is tightly modulated by moisture fluctuations and posited the moisture mode theory to explain its behavior. Here, we show that no climate model can realistically reproduce the moist thermodynamics of the MJO, particularly its sensitivity to humidity anomalies. The models that most reproduce the MJO's moist thermodynamics simulate a stronger MJO, and are generally more realistic.

1. Introduction

The Madden-Julian Oscillation (MJO; Madden & Julian, 1971, 1972) is a planetary-scale envelope of convection that is coupled with the circulation and moisture (Adames & Kim, 2016; Raymond & Fuchs, 2009; Sobel & Maloney, 2013, among others). This convective envelope often initiates over the Indian Ocean and propagates eastward at about 3–7 m s^{-1} (Rushley et al., 2022; C. Zhang & Ling, 2017). The MJO affects weather and climate around the globe through its teleconnections, including Asia and Australian rainfall events (Bagtasa, 2020; Chang et al., 2021; Cowan et al., 2022; Dao et al., 2023), tropical cyclone genesis (Chen et al., 2018; Rahul et al., 2022), El Niño Southern Oscillation and Atlantic Niño (Hendon et al., 2007; S.-K. Lee et al., 2023), as well as heatwaves and the frequency of tornadoes and hailstorms in the Northern America (Y.-Y. Lee & Grotjahn, 2019; Miller et al., 2022). In part due to these impacts, many studies in the last decades have tried to better understand the MJO through a combination of observation, theory, and modeling experiments (e.g., Adames & Kim, 2016; Maloney et al., 2010; Raymond & Fuchs, 2009; Sobel & Maloney, 2012; Wang et al., 2016, and references therein).

Numerous studies have observed that the growth of MJO convection is associated with feedbacks that increase moisture anomalies (Del Genio & Chen, 2015; Sobel et al., 2014; B. Zhang et al., 2019). Moreover, the eastward propagation of MJO is predominantly governed by horizontal and vertical moisture advection (Adames & Wallace, 2015; Hung & Sui, 2018; Kim, Kug, & Sobel, 2014; Kiranmayi & Maloney, 2011; K.-C. Tseng et al., 2015). These features have led to a view of MJO that is known as moisture mode theory. Moisture mode theory posits that the MJO precipitation is tightly modulated and organized by moisture fluctuations, while temperature anomalies play a minor role because of weak temperature gradient (WTG) balance (Adames, 2017; Adames & Kim, 2016; Adames & Maloney, 2021; Ahmed et al., 2021; Emanuel et al., 1994; Mayta & Adames Corraliza, 2023; Raymond & Fuchs, 2009; Sobel et al., 2014, among others). The processes that lead to evolution of the moisture fluctuations also lead to the evolution of moisture mode. These features led Ahmed et al. (2021) to propose three criteria to assess whether a wave is a moisture mode. Mayta et al. (2022) modified these criteria in order to apply them diagnostically to observations, reanalysis, and model output. The first criterion emphasizes a

19448007, 2024, 8, Downloaded from https://agupubs.onlinelibrary.wiley.com/doi/10.1029/2023GL106693, Wiley Online Library on [31/12/2024]. See the Terms and Conditions (https://onlinelibrary.wiley.com/terms-and-conditions) on Wiley Online Library for rules of use; OA articles are governed by the applicable Creative Commons License

high correlation between precipitation and column moisture. The second criterion describes that the wave behavior should satisfy WTG balance. The third criterion assures the dominance of moisture in the evolution of anomalous column moist static energy (MSE). Mayta et al. (2022) also included a fourth criterion based on the scale analysis of Adames et al. (2019) and Adames (2022). By using these criteria, Mayta and Adames Corraliza (2023) found that the MJO behaves as a moisture mode only over the Indian Ocean. Outside this region, temperature fluctuations are as influential as moisture anomalies in MJO's thermodynamics because its faster propagation prevents WTG balance.

Although our understanding of the MJO has significantly improved, accurate representation of MJO variability remains a major challenge in global climate models (GCMs; Ahn et al., 2017, 2020; Kim et al., 2009). It is well-documented that the failure of models to simulate the MJO is largely a result of inadequate treatment of deep cumulus convection, particularly its insufficient sensitivity to free tropospheric water vapor (e.g., Holloway et al., 2013; Kim, Lee, et al., 2014; M.-I. Lee et al., 2003; Maloney & Hartmann, 2001). Models in which convection is sensitive to water vapor fluctuations produce regions of precipitation that persist at the intraseasonal timescale, hence producing MJO activity. From this, models that have a strong coupling of precipitation with moisture can simulate more realistic MJO convection (Ahn et al., 2017; Holloway et al., 2013). Furthermore, a strong horizontal gradient of mean state moisture can drive robust MJO propagation (Ahn et al., 2020; Jiang, 2017). All of these features are consistent with the MJO being at least partially explained as a moisture mode.

Based on these previous results, we hypothesize that the moisture mode properties of the MJO are essential for its realistic simulation. To this end, we seek to examine the MJO simulation in the Coupled Model Intercomparison Project Phase 6 (CMIP6) models based on the moisture mode framework (Ahmed et al., 2021; Mayta et al., 2022; Mayta & Adames, 2023). Specifically, we seek to answer the following questions

Q1: Can the global climate models reproduce the MJO moisture mode properties over the Indian Ocean?
Q2: If a model can capture the moisture mode behaviors, does it mean that the model has better skills in the MJO simulation than others?

The structure of this paper is as follows. Section 2 describes the datasets and methods. Section 3 diagnoses MJO simulation by the moisture mode theory. In Section 4, we compare the good and poor simulations in the moisture mode behaviors against the observations. Section 5 discusses the relationship between the moisture mode criteria and MJO strength. Major findings are summarized in Section 6.

2. Data Description, Processing, and Diagnostics

2.1. Data Sources

Twenty-five CMIP6 models (Eyring et al., 2016) are adopted to evaluate MJO simulation in the 20-year (1995–2014) historical scenario (Table S1 in Supporting Information S1). We primarily use r1i1p1f1 ensemble member for most models, except for EC-Earth3 (r3i1p1f1), HadGEM3-GC31-LL (r1i1p1f3), HadGEM3-GC31-MM (r3i1p1f3), and UKESM1-0-LL (r1i1p1f2) based on their available data. Models that cannot provide all radiative fluxes to compute net radiation within the atmosphere are marked with asterisks (*).

Observation and reanalysis data are used as a reference for model simulations. We use the moisture, precipitation, temperature, horizontal winds, vertical velocity, geopotential height, radiation, and surface fluxes from the fifth generation of the European Center for Medium-Range Weather Forecasts (ECMWF) reanalysis (ERA5; Hersbach et al., 2019). The outgoing longwave radiation (OLR) from NOAA Physical Sciences Laboratory (Liebmann & Smith, 1996) is used to calculate the MJO index. The precipitation from Tropical Rainfall Measuring Mission (TRMM; Kummerow et al., 2000) product is applied to compute the realistic wave responses by the space-time power spectra. All data are interpolated into a uniform horizontal resolution of 2.5° longitude × 2.5° latitude. We discuss the MJO activity during the extended boreal winter (November–April) when the MJO is more active (X. Li et al., 2020; Q. Zhang et al., 2019).

2.2. Filtering, EOF Analysis, and Regressions

The dominant mode of the MJO convection is derived through empirical orthogonal function (EOF) analysis of 20–96-day bandpass filtered OLR over the equatorial belt (15°S–15°N). The first EOF mode (EOF1) has the

19448007, 2024, 8, Downloaded from https://agupubs.onlinelibrary.wiley.com/doi/10.1029/2023GL106693, Wiley Online Library on [31/12/2024]. See the Terms and Conditions (https://onlinelibrary.wiley.com/terms-and-conditions) on Wiley Online Library for rules of use; OA articles are governed by the applicable Creative Commons License

largest amplitude around 90°E (Figure S1 in Supporting Information S1). The field variables are lag regressed onto the first principal component (PC1) time series to obtain a composite of the MJO evolution from −30 to 30 days, following the same process as previous studies (e.g., Adames et al., 2021; Mayta & Adames Corraliza, 2023; Mayta et al., 2021). These perturbations are then scaled to one standard deviation (SD) of PC1. To make the peak MJO convection near 90°E occur at lag 0 day in all data, we refer to the basis function approach (J. Lee et al., 2019; Orbe et al., 2020, among others) to project simulated OLR anomalies onto the observed EOF1 and hence obtain the PC1 time series of each model.

2.3. Diagnostic Criteria

In order to evaluate the moist thermodynamics of simulated MJO, we apply the moisture mode criteria over the Indian Ocean (10°S–10°N, 75°E–100°E) region, where the MJO shows characteristics of a moisture mode (Mayta & Adames Corraliza, 2023). The criteria are (Ahmed et al., 2021; Mayta et al., 2022):

1. *Wave must exhibit a large moisture signature that is highly correlated with the precipitation anomalies*
   To be considered a moisture mode, the MJO's precipitation anomalies P' should be sensitive to column water vapor variations $\langle q\rangle'$. In other words, it must exhibit a high linear correlation between $\langle q\rangle'$ and P' ($R_{P,q}$) as follows,

$$\langle q\rangle' \propto P' \tag{1}$$

   where $\langle\cdot\rangle \equiv \frac{1}{g}\int_{100}^{1000}(\cdot)dp$ is vertical integration from 1,000 to 100 hPa, and primes ($'$) represent the regressed anomalies. The correlation coefficient between $\langle q\rangle'$ and P' should be higher than 0.9, indicating that the moisture fluctuations significantly modulate the precipitation evolution, at least 81% of the variance. The slope of $\langle q\rangle'$ to P' is the convective moisture adjustment time scale $\left(\tau_c \equiv \frac{\langle q\rangle'}{P'}\right)$, defined as the time to remove column moisture through rainfall (Bretherton et al., 2004). The τ_c of MJO convection should be about 1 day over the Indian Ocean (Mayta & Adames Corraliza, 2023).
2. *The system must be in the WTG balance*
   The WTG approximation states that the vertical advection of dry static energy (DSE) $\langle\omega\partial_p s\rangle'$ must approximate balance the apparent heat source $\langle Q_1\rangle'$:

$$\langle\omega\partial_p s\rangle' \simeq \langle Q_1\rangle' \tag{2}$$

   where $s{=}C_pT + gz$ is DSE. To satisfy this second criterion, the slope of $\langle Q_1\rangle'$ to $\langle\omega\partial_p s\rangle'$ should be close to 1 in linear least-squares fitting, and their correlation must also be higher than 0.9.

However, the second criterion might not confirm that temperature fluctuations are negligibly small. It could mean that apparent heat source is very large compared to the temperature tendency. To rigorously verify that moisture anomalies play a key role in modulating the system, the following third criterion is necessary.

3. *Moisture must govern the evolution of MSE*
   If the MJO is a moisture mode, the column water vapor must be the main contributor to its MSE (m),

$$\langle m\rangle' = \langle s\rangle' + \langle L_v q\rangle' \approx \langle L_v q\rangle' \tag{3}$$

   To guarantee the approximation in Equation 3, a slope of $\langle L_v q\rangle'$ to $\langle m\rangle'$ must be ∼1 in linear least-squares fitting ($S_{q,m}$), with a high correlation between both variables (>0.9).
4. N_{mode}
   The dimensionless N_{mode} parameter is also adopted to quantify the relative importance of column water vapor versus temperature in the evolution of MSE (Adames et al., 2019). N_{mode} is defined as in Adames et al. (2019) and Mayta et al. (2022) as:

$$N_{mode} \simeq \frac{c_p^2\tau}{c^2\tau_c} \tag{4}$$

19448007, 2024, 8, Downloaded from https://agupubs.onlinelibrary.wiley.com/doi/10.1029/2023GL106693, Wiley Online Library on [31/12/2024]. See the Terms and Conditions (https://onlinelibrary.wiley.com/terms-and-conditions) on Wiley Online Library for rules of use; OA articles are governed by the applicable Creative Commons License

where $c = 50$ m s^{-1} is the phase speed of a first baroclinic free gravity wave, c_p is the phase speed of MJO over the warm pool Indian Ocean, τ_c is the convective moisture adjustment time scale, and τ is the characteristic temporal scale of MJO (i.e., ∼37 days in the ERA5). The MJO can be classified as a moisture mode when $N_{mode} \ll 1$ (i.e., $\log_{10}N_{mode} < -0.5$).

Following Mayta et al. (2022), the first three criteria are applied to the reanalysis by constructing scatterplots of regressed field variables (Figure S2 in Supporting Information S1), considering time series from lag day −30 to day +30 and all grid points within the analysis domain (10°S–10°N, 75°E–100°E). Various methods exist to calculate τ_c, in addition to the one proposed in this study (e.g., Jiang et al., 2016). However, we have verified that the main findings of this study are not affected by the method used to calculate τ_c. For the fourth criterion, the c_p is estimated by applying the Radon Transform method (Mayta et al., 2024; Radon, 1917), which is described in Supporting Information S1. The same procedures are repeated for CMIP6 data.

3. Moist Thermodynamic Diagnostics of MJO Simulation

The moisture mode criteria applied to the reanalysis and models are summarized in Figure 1. Reanalysis, as recently documented in Mayta and Adames Corraliza (2023), shows a high correlation between $\langle q \rangle'$ and P' over the Indian Ocean ($R_{P,q} = 0.95$), whereas the climate models depict an average value of 0.88 ± 0.05. Among them, HadGEM3-GC31-LL, KACE-1-0-G, and TaiESM1 models have the highest correlation ($R_{P,q} = 0.94$). The remaining 15 models underestimate $R_{P,q}$ (<0.9; black values). The τ_c of ERA5 is about 1.02 days. Ten out of 25 models (40% of total) are within ±0.5 model SD relative to the reanalysis (0.93–1.12 days). For the WTG approximation, the slope of $\langle Q_1 \rangle'$ versus $\langle \omega \partial_p s \rangle'$ in reanalysis is 0.99 (not shown). The values of the 25 models range from 0.98 to 1.06, and the multi-model mean is 1.01 ± 0.02. The correlation between $\langle Q_1 \rangle'$ and $\langle \omega \partial_p s \rangle'$ is higher than 0.99 in ERA5 and all models included. It suggests that these simulations largely satisfy WTG balance over the Indian Ocean, so this criterion is not shown in Figure 1. $S_{q,m}$ in ERA5 is approximately 0.98 (Figure 1). The mean of the 25 models is ∼0.92 ± 0.06, with most models showing values ranging from 0.89 to 1.02 (within 1.5 SD relative to ERA5). However, the $S_{q,m}$ in 11 models is lower than 0.9, particularly the IITM-ESM and MPI-ESM-1-2-HAM models (<0.85). The relatively low $S_{q,m}$ values indicate that the contribution of $\langle s \rangle'$ to $\langle m \rangle'$ is more significant. All models and reanalysis have a high correlation coefficient (>0.98) between moisture and MSE anomalies (not shown).

The $\log_{10}N_{mode}$ value of ERA5 is approximately −0.69 ($N_{mode} \sim 0.2$), indicating that the MJO exhibits moisture mode behavior over the Indian Ocean, in agreement with Mayta and Adames Corraliza (2023). Eight models depict a $\log_{10}N_{mode} > -0.3$ ($N_{mode} > 0.5$), implying that their behavior is far from a moisture mode. It is worth noting that some models show reasonable results for the first three moisture mode criteria but have $\log_{10}N_{mode} > -0.25$ ($N_{mode} > 0.56$; e.g., ACCESS-CM2, HadGEM3-GC31-MM, and KACE-1-0-G). Adames et al. (2019) and Adames (2022) performed a scale analysis and demonstrated that N_{mode} is largely determined by the phase speed of the wave. These models, as expected, simulate a faster MJO phase speed ($c_p > 8$ m s^{-1}) than ERA5 (Figure S3 in Supporting Information S1). A high sensitivity of N_{mode} to c_p was found in these 25 CMIP6 models (further discussion in the SI). On the other hand, the $\log_{10}N_{mode} < -0.8$ ($N_{mode} < 0.16$; e.g., AWI-ESM-1-1-LR, IITM-ESM, IPSL-CM6A-LR-INCA, MPI-ESM-1-2-HAM, MPI-ESM1-2-HR, and MPI-ESM1-2-LR) are models with near stationary MJO-like behavior ($c_p < 2.2$ m s^{-1}).

For the simulated MJO to satisfy the moisture mode criteria, the model should have $R_{P,q} > 0.9$, $\tau_c \sim 1$ day (at least within ±0.5 model SD relative to the observation), $S_{q,m} > 0.9$, and that $\log_{10}N_{mode}$ ranges within −0.8 to −0.5 (marked by the blue values in Figure 1). The results show that no model accurately captures all the MJO's moisture mode properties seen in reanalysis. However, some models still have values reasonably close to the reanalysis but with a slightly long τ_c or small $S_{q,m}$.

4. Comparison Between Observations, Good, and Poor Models

In this section, we further discuss whether the models that capture the highest amount of moisture mode criteria are able to simulate a more realistic MJO. To this end, we consider relaxed standards to select relatively good and poor models. First, the $R_{P,q}$, τ_c, and $S_{q,m}$ of model range within ±1.5 SD relative to the reanalysis. Second, $\log_{10}N_{mode}$ should be −0.8 to −0.3 because $\log_{10}N_{mode} < -0.3$ ensures a higher contribution from the moisture fluctuation than the temperature fluctuation ($N_{mode} < 0.5$). In addition, we avoid selecting more than one model from the same research institution to prevent multi-model means being dominated by similar simulations. In cases

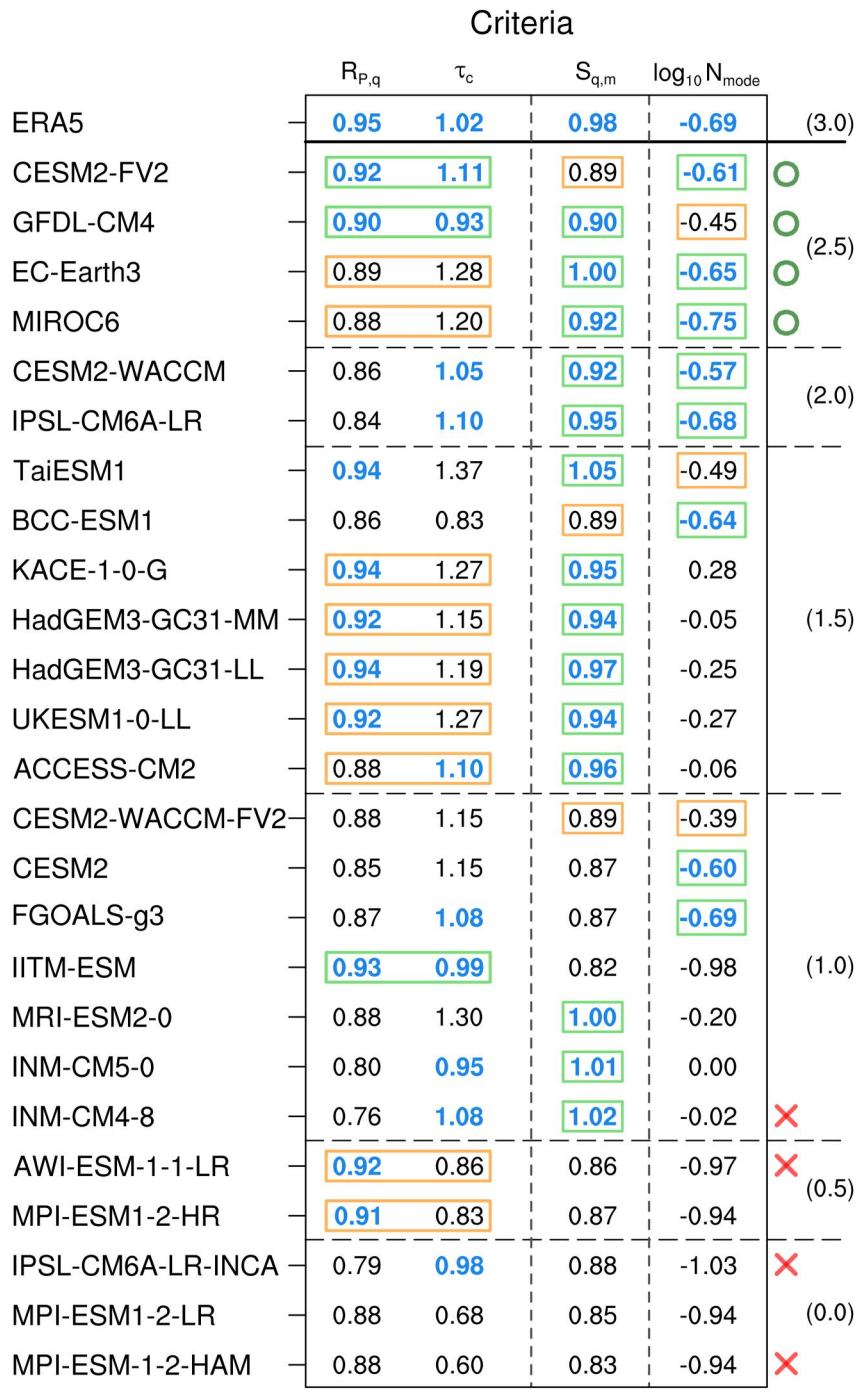

Figure 1. Values of criteria $R_{P,q}$, τ_c, $S_{q,m}$, and $\log_{10}N_{mode}$ from ERA5 and 25 Coupled Model Intercomparison Project Phase 6 models. Numbers in blue represent values that satisfy the moisture mode criteria: (1) $R_{P,q} > 0.9$, and τ_c within ±0.5 model standard deviations relative to ERA5 (0.93–1.12 days); (2) $S_{q,m} > 0.9$; and (3) $\log_{10}N_{mode}$ ranges from −0.8 to −0.5. Green boxes indicate that the model satisfies the moisture mode criteria ($R_{P,q}$ and τ_c considered as one) and receive a score of 1. Orange boxes represent that the model only satisfies the criteria for model selection (0.5 score): (1) $R_{P,q}$, τ_c, and $S_{q,m}$ range within ±1.5 model standard deviations relative to the reanalysis; and (2) $\log_{10}N_{mode}$ ranges from −0.8 to −0.3. Numbers in brackets denote the model's total scores. The relatively good and poor models are marked by the green circles and red crosses, respectively.

where models originate from the same research center, we choose the model with the best (worst) performance to include in the relatively good (poor) model group. Subsequently, we qualitatively assess the model's proficiency in replicating moisture mode properties using these criteria. For each criterion, the model is assigned a score of

19448007, 2024, 8, Downloaded from https://agupubs.onlinelibrary.wiley.com/doi/10.1029/2023GL106693, Wiley Online Library on [31/12/2024]. See the Terms and Conditions (https://onlinelibrary.wiley.com/terms-and-conditions) on Wiley Online Library for rules of use; OA articles are governed by the applicable Creative Commons License

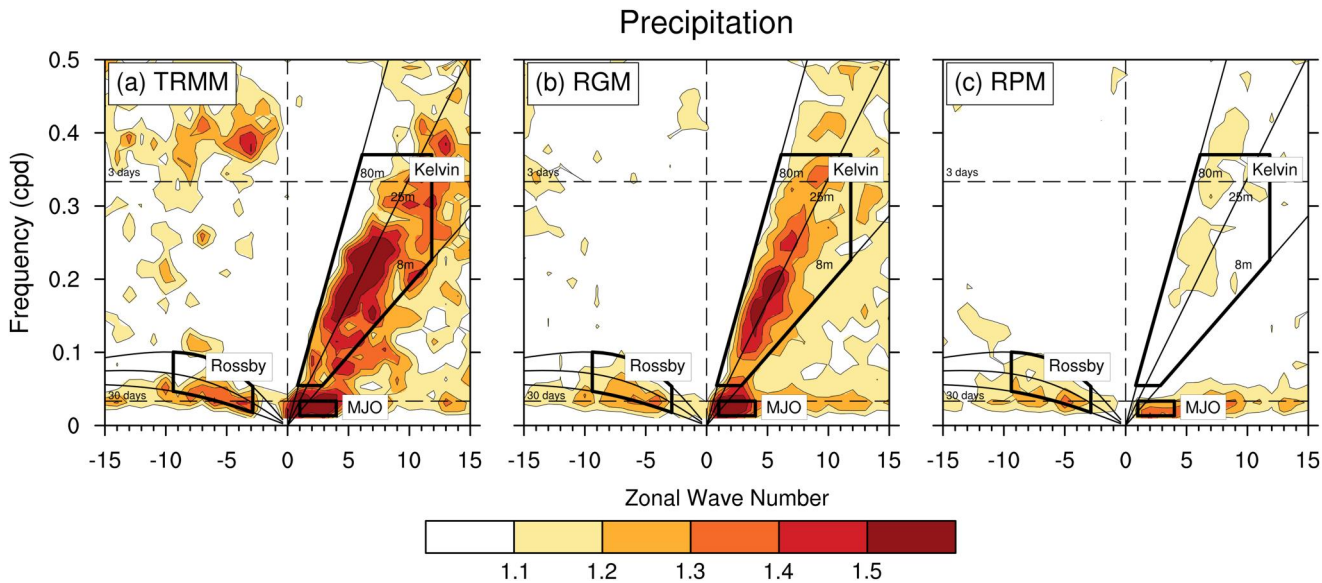

Figure 2. Space-time spectrum of the precipitation averaged between 10°S and 10°N for (a) Tropical Rainfall Measuring Mission, (b) the RGMs ensemble, and (c) the RPMs ensemble. The solid dispersion curves correspond to 8, 25, and 80 m equivalent depths. Color shading interval is 0.1. The functional form of the tapering window is the same as described in Wheeler and Kiladis (1999).

one if it successfully fulfills the criteria outlined in the moist thermodynamic diagnostics (green boxes in Figure 1). If the model only satisfies the relaxed criteria (orange boxes), it is assigned a score of 0.5. Models that fail the criteria receive a score of 0. Note that $R_{P,q}$ and τ_c are considered together as one criterion. Figure 1 shows the order of models sorted by their total score.

Based on the total scores, four relatively good models (RGMs; CESM2-FV2, EC-Earth3, GFDL-CM4, and MIROC6) are selected. For the relatively poor models (total score lower than 1), the IPSL-CM6A-LR-INCA, MPI-ESM-1-2-HAM, and AWI-ESM-1-1-LR are selected first. We adopt the MPI-ESM-1-2-HAM rather than MPI-ESM1-2-LR or MPI-ESM1-2-HR because the former has worse values in τ_c and $S_{q,m}$ than the latter. The INM-CM4-8 model stands out from the seven models (total score equal to 1) due to its relatively low moisture-rainfall correlation and unphysically large $\log_{10}N_{mode}$. Thus, we select the four relatively poor models (RPMs; AWI-ESM-1-1-LR, INM-CM4-8, IPSL-CM6A-LR-INCA, and MPI-ESM-1-2-HAM).

4.1. Space-Time Spectrum

First, we compute space-time power spectra, making use of the fast Fourier transform. The calculation procedure is similar to those used by previous studies (e.g., Y. Li et al., 2022; Rushley et al., 2019; Wheeler & Kiladis, 1999, among others). We use precipitation from TRMM, RGMs, and RPMs as an input for the calculation. The results of TRMM and ERA5 are similar (not shown), although ERA5 (1995–2014) has a longer period than TRMM observation (1998–2014).

Figure 2 shows the symmetric power spectra of precipitation in the frequency-wavenumber domain. For the MJO band (wavenumber $k = 1 - 4$, and period of 30–90 days), TRMM and ensemble good models show strong spectra (power >1.5), whereas it is relatively weak in the poor model group (power <1.4). While precipitation exhibits a strong Kelvin wave signal in the observation and RGMs, such a signal is largely weak in the RPMs. Overall, the good model group can capture better wave signals and intensities than the poor model group.

4.2. Mean State

Previous studies have found that a realistic representation of the background MSE is critical for MJO simulation because the advection of mean-state MSE by the MJO winds dominates the MJO propagation (e.g., Ahn et al., 2020; Jiang, 2017; Ren et al., 2021, and others). On the other hand, the mean low-level easterlies in the western Pacific can be a barrier to eastward propagating MJO in the model simulation (Inness & Slingo, 2003; Inness et al., 2003). Thus, it is worthwhile to compare the mean-state column-integrated MSE and 850-hPa zonal

19448007, 2024, 8, Downloaded from https://agupubs.onlinelibrary.wiley.com/doi/10.1029/2023GL106693, Wiley Online Library on [31/12/2024]. See the Terms and Conditions (https://onlinelibrary.wiley.com/terms-and-conditions) on Wiley Online Library for rules of use; OA articles are governed by the applicable Creative Commons License

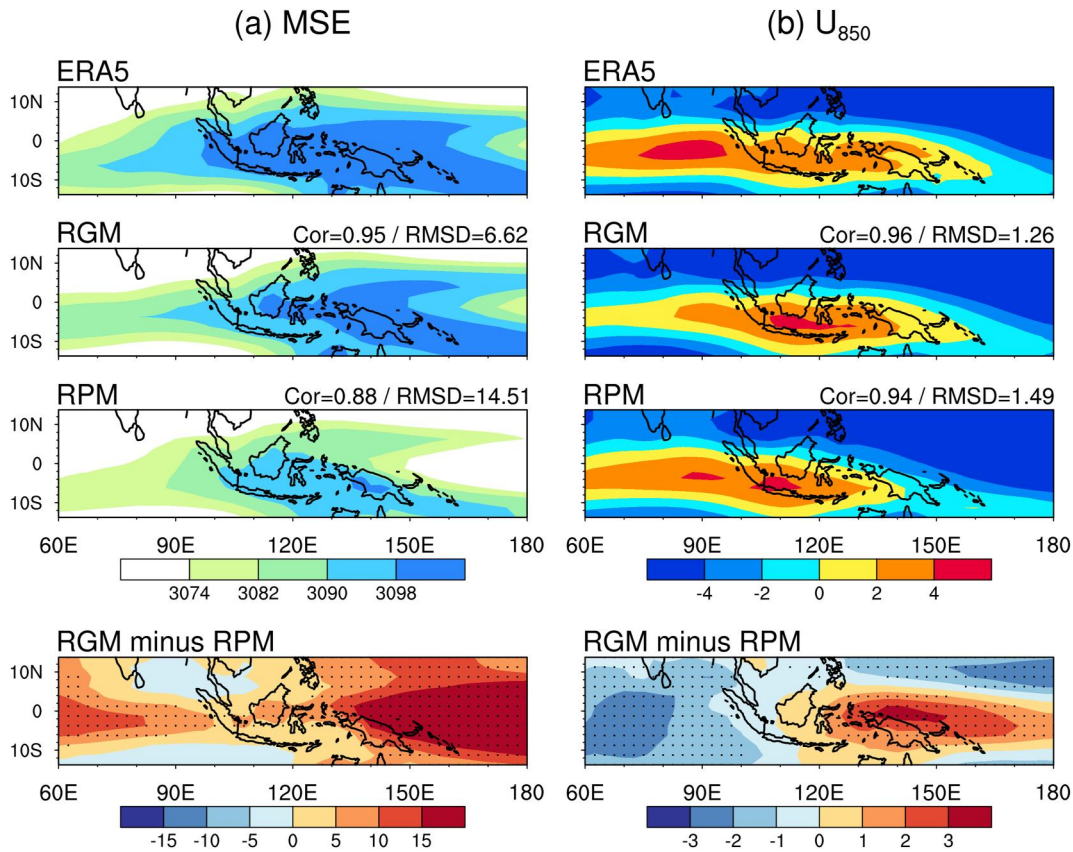

Figure 3. Spatial pattern of mean-state (a) column-integrated moist static energy (10^6 J m^{-2}) and (b) 850-hPa zonal wind (m s^{-1}) for the boreal winter, derived from (top) the ERA5 (middle top) ensemble good model (middle bottom) ensemble poor model group, and (bottom) the difference between RGM and RPM (RGM minus RPM). The gray dots in the bottom panels indicate statistical significance at the 95% confidence level. The pattern correlation (Cor)/root-mean-square deviation (root mean square deviation) between the model group and reanalysis is presented at the top-right corners, respectively.

winds between the reanalysis, RGM, and RPM (Figure 3). The pattern correlation and root mean square deviation between the individual model group and the reanalysis are also shown in the upper right corner of each panel in Figure 3.

For ERA5, the relatively high column MSE is concentrated over the Indo-Pacific warm pool and decreases with increasing latitude (Figure 3a). Most models simulate a similar but underestimated column MSE distribution compared with the reanalysis (not shown). The RGM has a higher column MSE over the equatorial warm pool relative to the RPM, especially in the western Pacific with the MSE extreme. This leads to stronger background zonal and meridional gradients of MSE in the good model group than in the poor model group. The observed westerlies cover the tropical warm pool from 60°E to 165°E, while the maximum wind speed occurs in the Indian Ocean (Figure 3b). For the RGM, the peak of zonal winds appears near the Maritime Continent, resulting in weaker westerlies over the Indian Ocean than reanalysis. In addition, the RGM simulates weaker (stronger) westerlies than the poor model group in the Indian Ocean (western Pacific) region. The westerlies can extend toward 150°E in the RGM; however, they are replaced by the easterly winds at 140°E in the RPM, especially for AWI-ESM-1-1-LR, INM-CM4-8 and IPSL-CM6A-LR-INCA (not shown), where the strong mean low-level easterlies might partially explain why their MJO convection cannot propagate across the Maritime Continent (Figure S3 in Supporting Information S1).

4.3. MSE Budget Analysis

The column-integrated MSE budget is widely used to investigate the moist energy recharging and discharging associated with MJO convection (Inoue & Back, 2015; Ren et al., 2021; W.-L. Tseng et al., 2022, and others). It is written as:

19448007, 2024, 8, Downloaded from https://agupubs.onlinelibrary.wiley.com/doi/10.1029/2023GL106693, Wiley Online Library on [31/12/2024]. See the Terms and Conditions (https://onlinelibrary.wiley.com/terms-and-conditions) on Wiley Online Library for rules of use; OA articles are governed by the applicable Creative Commons License

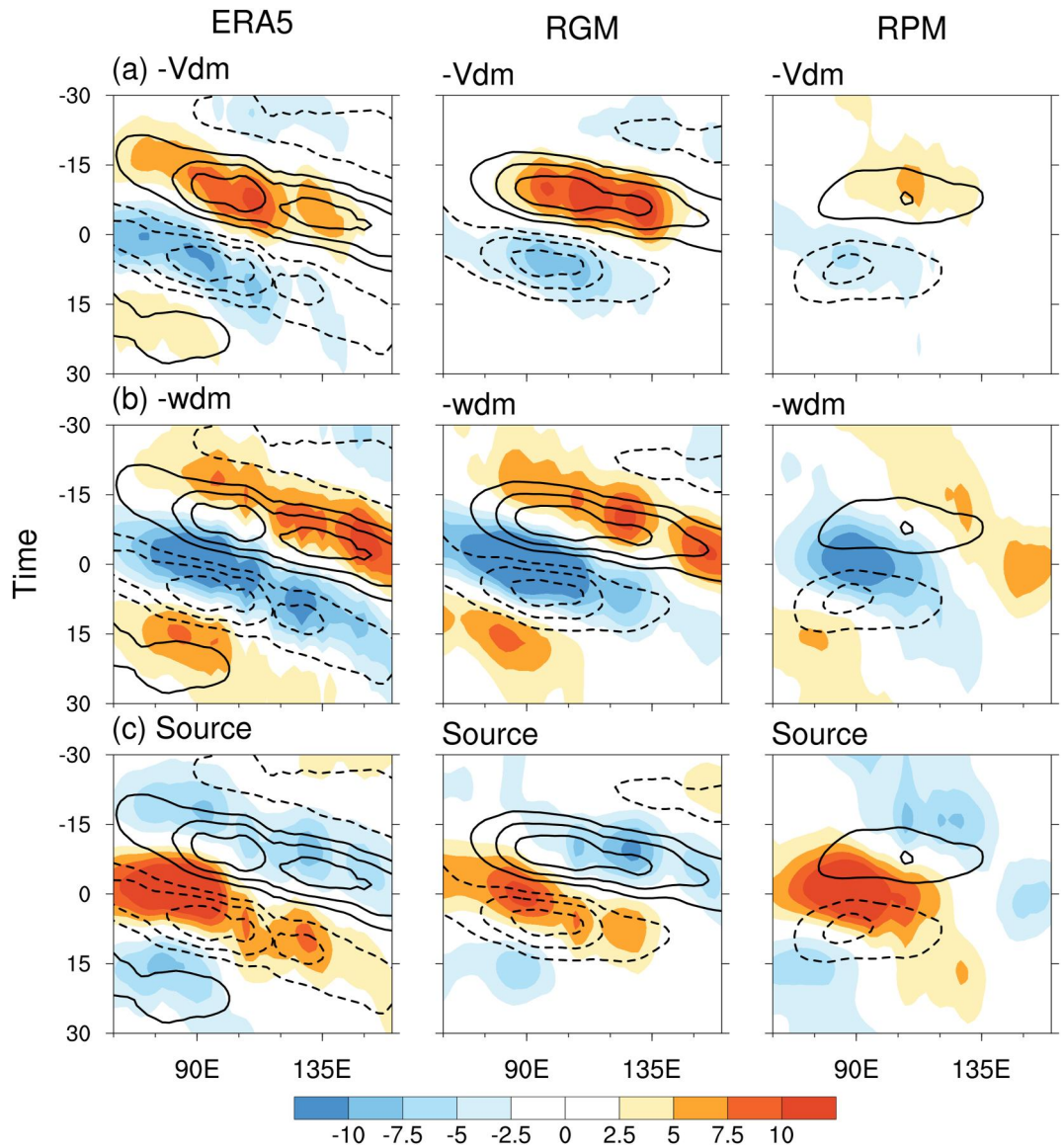

Figure 4. Hovmöller diagram of regressed moist static energy budget terms (shading) and $\langle \partial_t m \rangle'$ (contour) averaged between 10°S and 10°N from −30 to 30 days for the ERA5 (left panel), RGM (middle panel), and RPM (right panel). The individual terms are (a) $\langle -\mathbf{v} \cdot \nabla m \rangle'$, (b) $\langle -\omega \partial_p m \rangle'$, and (c) *Source*′. The contour and shading intervals are 2 and 2.5 W m^{-2}, respectively.

$$\langle \partial_t m \rangle' = \langle -\mathbf{v} \cdot \nabla m \rangle' + \langle -\omega \partial_p m \rangle' + Source' \tag{5}$$

where the left-side term in Equation 5 is the MSE tendency. The first and second terms on the right-side represent the horizontal and vertical MSE advection, respectively. The last term in Equation 5 are the MSE sources and sinks ($Source' = \langle Q_r \rangle' + L_v E' + SH'$) including the column radiative heating $\langle Q_r \rangle'$, surface latent heat flux $L_v E'$, and surface sensible heat flux SH'.

Figure 4 shows the Hovmöller diagram of the regressed MSE budget terms in Equation 5 for the ERA5 and model groups. $\langle -\mathbf{v} \cdot \nabla m \rangle'$ varies in phase with $\langle \partial_t m \rangle'$ (Figure 4a). RGM simulations reproduce the eastward MJO convection with strong $\langle -\mathbf{v} \cdot \nabla m \rangle'$ and $\langle \partial_t m \rangle'$. The RPM exhibits weak and nearly non-propagating convection. In Figure 4b, $\langle -\omega \partial_p m \rangle'$ starts moistening/drying the column energy before the positive/negative $\langle \partial_t m \rangle'$. Compared with ERA5, $\langle -\omega \partial_p m \rangle'$ has a stronger drying effect ($\langle -\omega \partial_p m \rangle' < 0$) in the RGM and an underestimated

19448007, 2024, 8, Downloaded from https://agupubs.onlinelibrary.wiley.com/doi/10.1029/2023GL106693, Wiley Online Library on [31/12/2024]. See the Terms and Conditions (https://onlinelibrary.wiley.com/terms-and-conditions) on Wiley Online Library for rules of use; OA articles are governed by the applicable Creative Commons License

19448007, 2024, 8, Downloaded from https://agupubs.onlinelibrary.wiley.com/doi/10.1029/2023GL106693, Wiley Online Library on [31/12/2024]. See the Terms and Conditions (https://onlinelibrary.wiley.com/terms-and-conditions) on Wiley Online Library for rules of use; OA articles are governed by the applicable Creative Commons License

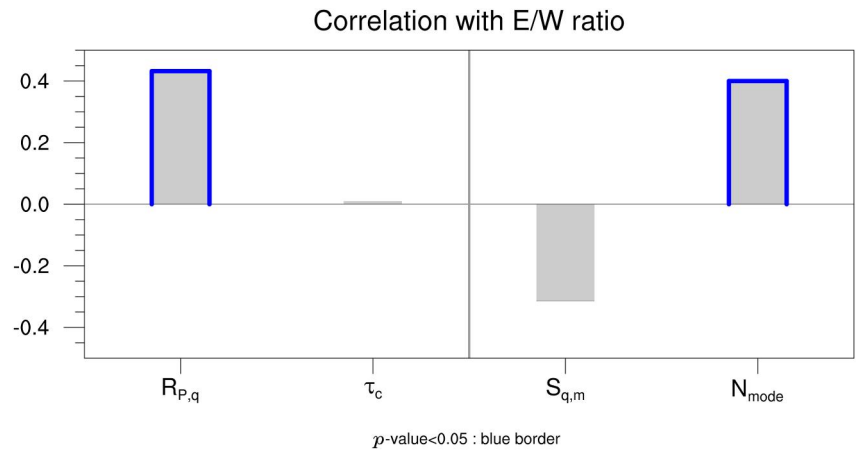

Figure 5. Inter-model comparison between the E/W ratio and $R_{P,q}$, τ_c, $S_{q,m}$, and N_{mode}. To calculate the correlation with the E/W ratio, the model results of $R_{P,q}$ and τ_c are used, while the absolute differences (i.e., |model minus observation|) of $S_{q,m}$ and N_{mode} are considered. Blue borders indicate correlations exceeding 95% confidence level (p-value <0.05).

amplitude in the RPM. The observed *Source′* exhibits a lagged evolution with $\langle \partial_t m \rangle'$ (Figure 4c). This feature implies that *Source′* is in phase with the column MSE anomalies rather than $\langle \partial_t m \rangle'$ and thus mainly contributes to the MJO maintenance. The simulated *Source′* of RGM is weaker than the reanalysis, whereas the *Source′* in the RPM does not show clear eastward propagation.

5. Relationship Between the Moisture Mode Criteria and MJO Strength

From an examination of Figure 2, we see that the RGMs exhibit a stronger MJO signal than the RPMs. Given that none of the four criteria directly diagnose MJO amplitude, this result should be examined in detail. Thus, we further compare the four moisture mode criteria with the east-west power ratio (E/W ratio). The E/W ratio assesses the MJO intensity by calculating the power ratio of eastward- and westward-propagating signals (periods of 30–60 days and wavenumbers 1–3) based on the power spectrum of OLR over the tropical region (a detailed explanation is presented in Section S4 of Supporting Information S1).

In Figure 5, $R_{P,q}$ has a high correlation with the E/W ratio, indicating that the models with higher coupling of precipitation and moisture simulate a stronger MJO. In contrast, τ_c does not show a significant correlation with the E/W ratio. This result is at odds with Jiang et al. (2016), in which models with a stronger amplitude of MJO precipitation generally have a shorter τ_c. This discrepancy may be methodological since Jiang et al. (2016) used rainfall anomalies over the warm pool rather than the E/W ratio to diagnose MJO amplitude.

For $S_{q,m}$ and N_{mode}, we compare the absolute values of the difference between the model value and the reanalysis (e.g., $|S_{q,m}(model) - S_{q,m}(ERA5)|$), with the E/W ratio. The results reveal a statistically-significant correlation between N_{mode} and the E/W ratio. Since N_{mode} is sensitive to the MJO phase speed (Figure S5 in Supporting Information S1), this result indicates that models with realistic MJO propagation also exhibit a stronger MJO amplitude. We also found that the models that most accurately capture the MJO's moisture mode behavior exhibit more realistic MJO intensity and periodicity (further discussion is presented in Section S4 of Supporting Information S1).

6. Summary and Conclusions

In this study, we applied the moisture mode theory-based diagnosis proposed by Ahmed et al. (2021), Mayta et al. (2022), and Mayta and Adames Corraliza (2023) to assess the moisture mode properties of MJO over the Indian Ocean (10°S–10°N, 75°E–100°E) in the 25 CMIP6 models. The following are answers to the two questions based on the results in Sections 3 to 4.

19448007, 2024, 8, Downloaded from https://agupubs.onlinelibrary.wiley.com/doi/10.1029/2023GL106693, Wiley Online Library on [31/12/2024]. See the Terms and Conditions (https://onlinelibrary.wiley.com/terms-and-conditions) on Wiley Online Library for rules of use; OA articles are governed by the applicable Creative Commons License

Q1: Can the global climate models reproduce the MJO moisture mode properties over the Indian Ocean?

Our results demonstrate that none of the models used in this study can reliably reproduce all moist thermodynamic properties of the MJO as observed in Figure 1: (a) Few models showed a high correlation (greater than 0.9) between moisture and precipitation anomalies and exhibited convective adjustment time scale (τ_c) that aligned with the reanalysis; (b) all models can satisfy the criteria for WTG balance; (c) nevertheless, 11 models still exhibited an unrealistically high contribution from temperature fluctuations to the MSE anomalies; and (d) limited number of models showed values of N_{mode} that are close to those of the reanalysis data. High values of N_{mode} ($\gg$0.5; $\log_{10}N_{mode} > -0.3$) or low N_{mode} ($\ll$0.16; $\log_{10}N_{mode} < -0.8$) imply that many models showed unrealistically fast or nearly non-propagating MJO convection, respectively (Figure S3 in Supporting Information S1). We also considered the analysis and procedures based on the model's EOF (Figure S6 in Supporting Information S1) rather than the observed EOF. However, these 25 models still do not demonstrate the moisture mode properties of the MJO (more details in Figure S7 and Section S3 of Supporting Information S1).

Q2: If a model can capture the moisture mode behaviors, does it mean that the model has better skills in the MJO simulation than others?

While no model fully captures the moisture mode behavior of the MJO, there is a subset that performs reasonably well. These good models (e.g., CESM2-FV2, EC-Earth3, GFDL-CM4, and MIROC6) show a stronger MJO signal than the relatively poor models (Figure 2). The good model group realistically simulates the mean-state column MSE and low-level zonal winds (Figure 3). The MSE budget associated with the MJO is better represented in the good models compared to the poor models, especially in the MSE advection terms (Figure 4). Our results indicate that models accurately capturing the moisture mode behavior of the MJO over the Indian Ocean demonstrate improved simulation of the MJO.

Two of the moisture mode criteria (moisture-rainfall correlation and N_{mode}) also have a significant correlation with the east-west power ratio (Figure 5), which is commonly used to denote the MJO simulation skill in previous studies (e.g., Ahn et al., 2017; Lan et al., 2022; Y. Li et al., 2022; Orbe et al., 2020). A robust MJO propagation is correlated with a more humid mean state and with stronger horizontal moisture gradients, as well as more robust MJO wind anomalies (Ahn et al., 2020; Y. Li et al., 2022). This consistency is expected since many previous studies have obtained these results under the a-priori assumption that the MJO behaves as a moisture mode. In other words, many previous studies implicitly assume that the moisture mode criteria are always satisfied, and that good MJO models are those that best simulate the processes that lead to the destabilization and propagation of moisture modes. These include having stronger horizontal moisture gradients that lead to more robust propagation via horizontal moisture advection, convection that is more sensitive to moisture variations, and a small effective gross moist stability (e.g., Ahn et al., 2017, 2020; Benedict et al., 2014).

Our study extends upon previous work by showing that the expected moisture mode behavior only exists in models that more robustly simulate the MJO. Thus, the relatively good MJO models do not just simulate the processes that lead to the destabilization and propagation of moisture modes, they are also the models that best simulate the moisture mode behavior of the MJO over the Indian Ocean. Poorer models not only have weaker or non-propagating MJO-like variability, but this variability is inconsistent with moisture mode behavior. The models best capturing the MJO's moisture mode behavior over the Indian Ocean also yield more realistic results in previous MJO skill metrics (see Figure S8 and Section S4 in Supporting Information S1 for more details). Thus, simulating a MJO that behaves as a moisture mode over the Indian Ocean may be synonymous with simulating a realistic MJO, and the four criteria used here appear to be useful diagnostic tools for evaluating MJO simulation performance.

In spite of these findings, we cannot say whether simulating the moisture mode behavior is what causes the models to perform better. It may be related to more realistic convection representation, or a combination of other factors. More work is needed to better understand the causality.

Data Availability Statement

We downloaded the CMIP6 model simulation outputs from the Lawrence Livermore National Laboratory (https://esgf-node.llnl.gov/search/cmip6). The interpolated OLR data was obtained from the NOAA (https://psl.noaa.gov/data/gridded/data.olrcdr.interp.html). The precipitation from TRMM (3B42) dataset was downloaded

from the NASA (https://disc.gsfc.nasa.gov/). The reanalysis data was available at ECMWF (ERA5; https://doi.org/10.24381/cds.adbb2d47).

Acknowledgments
QJL was sponsored by the Ministry of Science and Technology of Taiwan under Grant MOST111-2917-I-008-002 and NSF CAREER Grant 2236433. VM and ÁFAC were also supported by NOAA Grant NA22OAR4310611 and NSF CAREER Grant 2236433.

References

Adames, Á. F. (2017). Precipitation budget of the Madden–Julian Oscillation. *Journal of the Atmospheric Sciences*, *74*(6), 1799–1817. https://doi.org/10.1175/jas-d-16-0242.1

Adames, Á. F. (2022). The basic equations under weak temperature gradient balance: Formulation, scaling, and types of convectively-coupled motions. *Journal of the Atmospheric Sciences*, *79*(8), 2087–2108. https://doi.org/10.1175/jas-d-21-0215.1

Adames, Á. F., & Kim, D. (2016). The MJO as a dispersive, convectively coupled moisture wave: Theory and observations. *Journal of the Atmospheric Sciences*, *73*(3), 913–941. https://doi.org/10.1175/jas-d-15-0170.1

Adames, Á. F., Kim, D., Clark, S. K., Ming, Y., & Inoue, K. (2019). Scale analysis of moist thermodynamics in a simple model and the relationship between moisture modes and gravity waves. *Journal of the Atmospheric Sciences*, *76*(12), 3863–3881. https://doi.org/10.1175/jas-d-19-0121.1

Adames, A. F., & Maloney, E. D. (2021). Moisture mode theory's contribution to advances in our understanding of the Madden-Julian Oscillation and other tropical disturbances. *Current Climate Change Reports*, *7*(2), 72–85. https://doi.org/10.1007/s40641-021-00172-4

Adames, Á. F., Powell, S. W., Ahmed, F., Mayta, V. C., & Neelin, J. D. (2021). Tropical precipitation evolution in a buoyancy-budget framework. *Journal of the Atmospheric Sciences*, *78*(2), 509–528. https://doi.org/10.1175/jas-d-20-0074.1

Adames, Á. F., & Wallace, J. M. (2015). Three-dimensional structure and evolution of the moisture field in the MJO. *Journal of the Atmospheric Sciences*, *72*(10), 3733–3754. https://doi.org/10.1175/jas-d-15-0003.1

Ahmed, F., Neelin, J. D., & Adames, Á. F. (2021). Quasi-equilibrium and weak temperature gradient balances in an equatorial beta-plane model. *Journal of the Atmospheric Sciences*, *78*(1), 209–227. https://doi.org/10.1175/jas-d-20-0184.1

Ahn, M.-S., Kim, D., Kang, D., Lee, J., Sperber, K. R., Gleckler, P. J., et al. (2020). MJO propagation across the Maritime Continent: Are CMIP6 models better than CMIP5 models? *Geophysical Research Letters*, *47*(11), e2020GL087250. https://doi.org/10.1029/2020gl087250

Ahn, M.-S., Kim, D., Sperber, K. R., Kang, I.-S., Maloney, E., Waliser, D., & Hendon, H. (2017). MJO simulation in CMIP5 climate models: MJO skill metrics and process-oriented diagnosis. *Climate Dynamics*, *49*(11), 4023–4045. https://doi.org/10.1007/s00382-017-3558-4

Bagtasa, G. (2020). Influence of Madden–Julian oscillation on the intraseasonal variability of summer and winter monsoon rainfall in the Philippines. *Journal of Climate*, *33*(22), 9581–9594. https://doi.org/10.1175/jcli-d-20-0305.1

Benedict, J. J., Maloney, E. D., Sobel, A. H., & Frierson, D. M. (2014). Gross moist stability and MJO simulation skill in three full-physics GCMs. *Journal of the Atmospheric Sciences*, *71*(9), 3327–3349. https://doi.org/10.1175/jas-d-13-0240.1

Bretherton, C. S., Peters, M. E., & Back, L. E. (2004). Relationships between water vapor path and precipitation over the tropical oceans. *Journal of Climate*, *17*(7), 1517–1528. https://doi.org/10.1175/1520-0442(2004)017<1517:rbwvpa>2.0.co;2

Chang, C.-H., Johnson, N. C., & Yoo, C. (2021). Evaluation of subseasonal impacts of the MJO/BSISO in the East Asian extended summer. *Climate Dynamics*, *56*(11), 3553–3568. https://doi.org/10.1007/s00382-021-05656-5

Chen, J.-M., Wu, C.-H., Chung, P.-H., & Sui, C.-H. (2018). Influence of intraseasonal–interannual oscillations on tropical cyclone genesis in the western North Pacific. *Journal of Climate*, *31*(12), 4949–4961. https://doi.org/10.1175/jcli-d-17-0601.1

Cowan, T., Wheeler, M. C., & Marshall, A. G. (2022). The combined influence of the Madden-Julian Oscillation and El Niño-Southern Oscillation on Australian rainfall. *Journal of Climate*, 1–44.

Dao, T. L., Vincent, C. L., & Lane, T. P. (2023). Multiscale influences on rainfall in northeast Australia. *Journal of Climate*, *36*(17), 5989–6006. https://doi.org/10.1175/jcli-d-22-0835.1

Del Genio, A. D., & Chen, Y. (2015). Cloud-radiative driving of the Madden-Julian Oscillation as seen by the A-Train. *Journal of Geophysical Research: Atmospheres*, *120*(11), 5344–5356. https://doi.org/10.1002/2015jd023278

Emanuel, K. A., David Neelin, J., & Bretherton, C. S. (1994). On large-scale circulations in convecting atmospheres. *Quarterly Journal of the Royal Meteorological Society*, *120*(519), 1111–1143. https://doi.org/10.1002/qj.49712051902

Eyring, V., Bony, S., Meehl, G. A., Senior, C. A., Stevens, B., Stouffer, R. J., & Taylor, K. E. (2016). Overview of the Coupled Model Intercomparison Project Phase 6 (CMIP6) experimental design and organization. *Geoscientific Model Development*, *9*(5), 1937–1958. https://doi.org/10.5194/gmd-9-1937-2016

Hendon, H. H., Wheeler, M. C., & Zhang, C. (2007). Seasonal dependence of the MJO–ENSO relationship. *Journal of Climate*, *20*(3), 531–543. https://doi.org/10.1175/jcli4003.1

Hersbach, H., Bell, B., Berrisford, P., Horányi, A., Sabater, J. M., Nicolas, J., et al. (2019). Global reanalysis: Goodbye ERA-Interim, hello ERA5. *ECMWF newsletter*, *159*, 17–24.

Holloway, C. E., Woolnough, S. J., & Lister, G. M. (2013). The effects of explicit versus parameterized convection on the MJO in a large-domain high-resolution tropical case study. Part I: Characterization of large-scale organization and propagation. *Journal of the Atmospheric Sciences*, *70*(5), 1342–1369. https://doi.org/10.1175/jas-d-12-0227.1

Hung, C.-S., & Sui, C.-H. (2018). A diagnostic study of the evolution of the MJO from Indian Ocean to Maritime Continent: Wave dynamics versus advective moistening processes. *Journal of Climate*, *31*(10), 4095–4115. https://doi.org/10.1175/jcli-d-17-0139.1

Inness, P. M., & Slingo, J. M. (2003). Simulation of the Madden–Julian Oscillation in a coupled general circulation model. Part I: Comparison with observations and an atmosphere-only GCM. *Journal of Climate*, *16*(3), 345–364. https://doi.org/10.1175/1520-0442(2003)016<0345:sotmjo>2.0.co;2

Inness, P. M., Slingo, J. M., Guilyardi, E., & Cole, J. (2003). Simulation of the Madden–Julian Oscillation in a coupled general circulation model. Part II: The role of the basic state. *Journal of Climate*, *16*(3), 365–382. https://doi.org/10.1175/1520-0442(2003)016<0365:sotmjo>2.0.co;2

Inoue, K., & Back, L. (2015). Column-integrated moist static energy budget analysis on various time scales during TOGA COARE. *Journal of the Atmospheric Sciences*, *72*(5), 1856–1871. https://doi.org/10.1175/jas-d-14-0249.1

Jiang, X. (2017). Key processes for the eastward propagation of the Madden-Julian Oscillation based on multimodel simulations. *Journal of Geophysical Research: Atmospheres*, *122*(2), 755–770. https://doi.org/10.1002/2016jd025955

Jiang, X., Zhao, M., Maloney, E. D., & Waliser, D. E. (2016). Convective moisture adjustment time scale as a key factor in regulating model amplitude of the Madden-Julian Oscillation. *Geophysical Research Letters*, *43*(19), 10–412. https://doi.org/10.1002/2016gl070898

Kim, D., Kug, J.-S., & Sobel, A. H. (2014). Propagating versus nonpropagating Madden–Julian Oscillation events. *Journal of Climate*, *27*(1), 111–125. https://doi.org/10.1175/jcli-d-13-00084.1

Kim, D., Lee, M.-I., Kim, D., Schubert, S. D., Waliser, D. E., & Tian, B. (2014). Representation of tropical subseasonal variability of precipitation in global reanalyses. *Climate Dynamics*, *43*(1–2), 517–534. https://doi.org/10.1007/s00382-013-1890-x

19448007, 2024, 8, Downloaded from https://agupubs.onlinelibrary.wiley.com/doi/10.1029/2023GL106693, Wiley Online Library on [31/12/2024]. See the Terms and Conditions (https://onlinelibrary.wiley.com/terms-and-conditions) on Wiley Online Library for rules of use; OA articles are governed by the applicable Creative Commons License

Kim, D., Sperber, K., Stern, W., Waliser, D., Kang, I.-S., Maloney, E., et al. (2009). Application of MJO simulation diagnostics to climate models. *Journal of Climate*, *22*(23), 6413–6436. https://doi.org/10.1175/2009jcli3063.1

Kiranmayi, L., & Maloney, E. D. (2011). Intraseasonal moist static energy budget in reanalysis data. *Journal of Geophysical Research*, *116*(D21), D21117. https://doi.org/10.1029/2011jd016031

Kummerow, C., Simpson, J., Thiele, O., Barnes, W., Chang, A., Stocker, E., et al. (2000). The status of the Tropical Rainfall Measuring Mission (TRMM) after two years in orbit. *Journal of Applied Meteorology*, *39*(12), 1965–1982. https://doi.org/10.1175/1520-0450(2001)040<1965:tsottr>2.0.co;2

Lan, Y.-Y., Hsu, H.-H., Tseng, W.-L., & Jiang, L.-C. (2022). Embedding a one-column ocean model in the Community Atmosphere Model 5.3 to improve Madden–Julian Oscillation simulation in boreal winter. *Geoscientific Model Development*, *15*(14), 5689–5712. https://doi.org/10.5194/gmd-15-5689-2022

Lee, J., Sperber, K. R., Gleckler, P. J., Bonfils, C. J., & Taylor, K. E. (2019). Quantifying the agreement between observed and simulated extratropical modes of interannual variability. *Climate Dynamics*, *52*(7), 4057–4089. https://doi.org/10.1007/s00382-018-4355-4

Lee, M.-I., Kang, I.-S., & Mapes, B. E. (2003). Impacts of cumulus convection parameterization on aqua-planet AGCM simulations of tropical intraseasonal variability. *Journal of the Meteorological Society of Japan. Ser. II*, *81*(5), 963–992. https://doi.org/10.2151/jmsj.81.963

Lee, S.-K., Lopez, H., Tuchen, F. P., Kim, D., Foltz, G. R., & Wittenberg, A. T. (2023). On the genesis of the 2021 Atlantic Niño. *Geophysical Research Letters*, *50*(16), e2023GL104452. https://doi.org/10.1029/2023gl104452

Lee, Y.-Y., & Grotjahn, R. (2019). Evidence of specific MJO phase occurrence with summertime California Central Valley extreme hot weather. *Advances in Atmospheric Sciences*, *36*(6), 589–602. https://doi.org/10.1007/s00376-019-8167-1

Li, X., Yin, M., Chen, X., Yang, M., Xia, F., Li, L., et al. (2020). Impacts of the tropical Pacific–Indian Ocean associated mode on Madden–Julian Oscillation over the Maritime Continent in boreal winter. *Atmosphere*, *11*(10), 1049. https://doi.org/10.3390/atmos11101049

Li, Y., Wu, J., Luo, J.-J., & Yang, Y. M. (2022). Evaluating the eastward propagation of the MJO in CMIP5 and CMIP6 models based on a variety of diagnostics. *Journal of Climate*, *35*(6), 1719–1743. https://doi.org/10.1175/jcli-d-21-0378.1

Liebmann, B., & Smith, C. A. (1996). Description of a complete (interpolated) outgoing longwave radiation dataset. *Bulletin of the American Meteorological Society*, *77*(6), 1275–1277.

Madden, R. A., & Julian, P. R. (1971). Detection of a 40–50 day oscillation in the zonal wind in the tropical Pacific. *Journal of the Atmospheric Sciences*, *28*(5), 702–708. https://doi.org/10.1175/1520-0469(1971)028<0702:doadoi>2.0.co;2

Madden, R. A., & Julian, P. R. (1972). Description of global-scale circulation cells in the tropics with a 40–50 day period. *Journal of the Atmospheric Sciences*, *29*(6), 1109–1123. https://doi.org/10.1175/1520-0469(1972)029<1109:dogscc>2.0.co;2

Maloney, E. D., & Hartmann, D. L. (2001). The sensitivity of intraseasonal variability in the NCAR CCM3 to changes in convective parameterization. *Journal of Climate*, *14*(9), 2015–2034. https://doi.org/10.1175/1520-0442(2001)014<2015:tsoivi>2.0.co;2

Maloney, E. D., Sobel, A. H., & Hannah, W. M. (2010). Intraseasonal variability in an aquaplanet general circulation model. *Journal of Advances in Modeling Earth Systems*, *2*(2). https://doi.org/10.3894/james.2010.2.5

Mayta, V. C., & Adames, Á. F. (2023). Moist thermodynamics of convectively coupled waves over the western hemisphere. *Journal of Climate*, *36*(9), 1–35. https://doi.org/10.1175/jcli-d-22-0435.1

Mayta, V. C., Adames, Á. F., & Ahmed, F. (2022). Westward-propagating moisture mode over the tropical western hemisphere. *Geophysical Research Letters*, *49*(6), e2022GL097799. https://doi.org/10.1029/2022gl097799

Mayta, V. C., & Adames Corraliza, Á. F. (2023). Is the Madden-Julian Oscillation a moisture mode? *Geophysical Research Letters*, *50*(15), e2023GL103002. https://doi.org/10.1029/2023gl103002

Mayta, V. C., Adames Corraliza, Á. F., & Lin, Q.-J. (2024). The Radon and Hilbert transforms and their applications to atmospheric waves. *Atmospheric Science Letters*, e1215. https://doi.org/10.1002/asl.1215

Mayta, V. C., Kiladis, G. N., Dias, J., Silva Dias, P. L., & Gehne, M. (2021). Convectively coupled Kelvin waves over tropical South America. *Journal of Climate*, *34*(16), 6531–6547. https://doi.org/10.1175/jcli-d-20-0662.1

Miller, D. E., Gensini, V. A., & Barrett, B. S. (2022). Madden-Julian Oscillation influences United States springtime tornado and hail frequency. *npj Climate and Atmospheric Science*, *5*(1), 1–8. https://doi.org/10.1038/s41612-022-00263-5

Orbe, C., Van Roekel, L., Adames, Á. F., Dezfuli, A., Fasullo, J., Gleckler, P. J., et al. (2020). Representation of modes of variability in six US climate models. *Journal of Climate*, *33*(17), 7591–7617. https://doi.org/10.1175/jcli-d-19-0956.1

Radon, J. (1917). Uber die bestimmung von funktionen durch ihre intergralwerte la'ngs gewisser mannigfaltikeiten. *Berichte uber die Verhandlungen Gesellshaft der Wissenschaften zu Leipzig*, *69*, 262–277.

Rahul, R., Kuttippurath, J., Chakraborty, A., & Akhila, R. (2022). The inverse influence of MJO on the cyclogenesis in the north Indian Ocean. *Atmospheric Research*, *265*, 105880. https://doi.org/10.1016/j.atmosres.2021.105880

Raymond, D. J., & Fuchs, Ž. (2009). Moisture modes and the Madden–Julian Oscillation. *Journal of Climate*, *22*(11), 3031–3046. https://doi.org/10.1175/2008jcli2739.1

Ren, P., Kim, D., Ahn, M.-S., Kang, D., & Ren, H.-L. (2021). Intercomparison of MJO column moist static energy and water vapor budget among six modern reanalysis products. *Journal of Climate*, *34*(8), 2977–3001. https://doi.org/10.1175/jcli-d-20-0653.1

Rushley, S. S., Janiga, M. A., Ridout, J. A., & Reynolds, C. A. (2022). The impact of mean state moisture biases on MJO skill in the Navy ESPC. *Monthly Weather Review*, *150*(7), 1725–1745. https://doi.org/10.1175/mwr-d-21-0225.1

Rushley, S. S., Kim, D., & Adames, Á. F. (2019). Changes in the MJO under greenhouse gas–induced warming in CMIP5 models. *Journal of Climate*, *32*(3), 803–821. https://doi.org/10.1175/jcli-d-18-0437.1

Sobel, A., & Maloney, E. (2012). An idealized semi-empirical framework for modeling the Madden–Julian Oscillation. *Journal of the Atmospheric Sciences*, *69*(5), 1691–1705. https://doi.org/10.1175/jas-d-11-0118.1

Sobel, A., & Maloney, E. (2013). Moisture modes and the eastward propagation of the MJO. *Journal of the Atmospheric Sciences*, *70*(1), 187–192. https://doi.org/10.1175/jas-d-12-0189.1

Sobel, A., Wang, S., & Kim, D. (2014). Moist static energy budget of the MJO during DYNAMO. *Journal of the Atmospheric Sciences*, *71*(11), 4276–4291. https://doi.org/10.1175/jas-d-14-0052.1

Tseng, K.-C., Sui, C.-H., & Li, T. (2015). Moistening processes for Madden–Julian oscillations during DYNAMO/CINDY. *Journal of Climate*, *28*(8), 3041–3057. https://doi.org/10.1175/jcli-d-14-00416.1

Tseng, W.-L., Hsu, H.-H., Lan, Y.-Y., Lee, W.-L., Tu, C.-Y., Kuo, P.-H., et al. (2022). Improving Madden–Julian Oscillation simulation in atmospheric general circulation models by coupling with a one-dimensional snow–ice–thermocline ocean model. *Geoscientific Model Development*, *15*(14), 5529–5546. https://doi.org/10.5194/gmd-15-5529-2022

Wang, B., Liu, F., & Chen, G. (2016). A trio-interaction theory for Madden–Julian Oscillation. *Geoscience Letters*, *3*(1), 1–16. https://doi.org/10.1186/s40562-016-0066-z

19448007, 2024, 8, Downloaded from https://agupubs.onlinelibrary.wiley.com/doi/10.1029/2023GL106693, Wiley Online Library on [31/12/2024]. See the Terms and Conditions (https://onlinelibrary.wiley.com/terms-and-conditions) on Wiley Online Library for rules of use; OA articles are governed by the applicable Creative Commons License

Wheeler, M., & Kiladis, G. N. (1999). Convectively coupled equatorial waves: Analysis of clouds and temperature in the wavenumber–frequency domain. *Journal of the Atmospheric Sciences*, *56*(3), 374–399. https://doi.org/10.1175/1520-0469(1999)056<0374:ccewao>2.0.co;2

Zhang, B., Kramer, R. J., & Soden, B. J. (2019). Radiative feedbacks associated with the Madden–Julian Oscillation. *Journal of Climate*, *32*(20), 7055–7065. https://doi.org/10.1175/jcli-d-19-0144.1

Zhang, C., & Ling, J. (2017). Barrier effect of the Indo-Pacific Maritime continent on the MJO: Perspectives from tracking MJO precipitation. *Journal of Climate*, *30*(9), 3439–3459. https://doi.org/10.1175/jcli-d-16-0614.1

Zhang, Q., Li, T., & Liu, J. (2019). Contrast of evolution characteristics of boreal summer and winter intraseasonal oscillations over tropical Indian Ocean. *Journal of Meteorological Research*, *33*(4), 678–694. https://doi.org/10.1007/s13351-019-9015-z

References From the Supporting Information

Waliser, D., Sperber, K., Hendon, H., Kim, D., Maloney, E., Wheeler, M., et al. (2009). MJO simulation diagnostics. *Journal of Climate*, *22*(11), 3006–3030.

Wheeler, M. C., & Hendon, H. H. (2004). An all-season real-time multivariate MJO index: Development of an index for monitoring and prediction. *Monthly Weather Review*, *132*(8), 1917–1932. https://doi.org/10.1175/1520-0493(2004)132<1917:aarmmi>2.0.co;2

Yang, G.-Y., Hoskins, B., & Slingo, J. (2007). Convectively coupled equatorial waves. Part II: Propagation characteristics. *Journal of the Atmospheric Sciences*, *64*(10), 3424–3437. https://doi.org/10.1175/jas4018.1

19448007, 2024, 8, Downloaded from https://agupubs.onlinelibrary.wiley.com/doi/10.1029/2023GL106693, Wiley Online Library on [31/12/2024]. See the Terms and Conditions (https://onlinelibrary.wiley.com/terms-and-conditions) on Wiley Online Library for rules of use; OA articles are governed by the applicable Creative Commons License